

Dependence of Kinematics on the Age of Stars in the Solar Neighborhood

G. A. Gontcharov*

July 9, 2018

Pulkovo Astronomical Observatory, Russian Academy of Sciences, Pulkovskoe sh. 65, St. Petersburg, 196140 Russia

Key words: HertzsprungRussell diagram; stellar kinematics; Galactic solar neighborhood.

The variations of kinematic parameters with age are considered for a sample of 15 402 thin-disk O–F stars with accurate α , δ , μ , and $\pi > 3$ mas from the Hipparcos catalogue and radial velocities from the PCRV catalogue. The ages have been calculated from the positions of the stars on the Hertzsprung–Russell diagram relative to the isochrones from the Padova database by taking into account the extinction from the previously constructed 3D analytical model and extinction coefficient R_V from the 3D map of its variations. Smooth, mutually reconciled variations of the velocity dispersions $\sigma(U)$, $\sigma(V)$, $\sigma(W)$, solar motion components U_\odot , V_\odot , W_\odot , Ogorodnikov–Milne model parameters, Oort constants, and vertex deviation l_{xy} consistent with all of the extraneous results for which the stellar ages were determined have been found. The velocity dispersion variations are well fitted by power laws the deviations from which are explained by the influence of predominantly radial stellar streams: Sirius, Hyades, α Cet/Wolf 630, and Hercules. The accuracy of determining the solar motion relative to the local standard of rest is shown to be fundamentally limited due to these variations of stellar kinematics. The deviations of our results from those of Dehnen and Binney (1998), the Geneva–Copenhagen survey of dwarfs, and the Besancon model of the Galaxy are explained by the use of PCRV radial velocities with corrected systematic errors.

*E-mail: georgegontcharov@yahoo.com

INTRODUCTION

Among the kinematic parameters of stars, the following parameters are most informative and are traditionally considered: the characteristics of the distribution of stars in the phase space of velocity components U , V , W in the Galactic coordinate system, their dispersions $\sigma(U)$, $\sigma(V)$, $\sigma(W)$, the parameters of the linear Ogorodnikov–Milne model, the related Oort constants A , B , C , K , and the components of the peculiar solar motion (motion toward the apex) relative to the local standard of rest (LSR). By the latter we mean an imaginary star or a reference point that is presently at the location of the Sun and moves uniformly in a circular orbit in the real gravitational potential of the Galaxy averaged over the Galactic longitude.

The estimates of kinematic parameters for different samples of stars are contradictory (see, e.g., Francis and Anderson 2009). This forces one to search for not just the age–velocity relation but their smooth, physically justified and reconciled (for different parameters) variations with stellar age.

Here, we calculate the components of the stellar positions and motions in the Galactic coordinate system (the positions in 6D space $XYZUVW$, the X axis is directed to the Galactic center, the Y axis is in the direction of Galactic rotation, and the Z axis is directed to the North Pole) for a sample of early-type main-sequence (MS) stars. We independently estimate the most probable ages of these stars, establish the variations of kinematics with age, and compare them with extraneous results.

COORDINATES AND VELOCITIES OF THIN-DISK STARS

The Pulkovo Compilation of Radial Velocities (PCRV, Gontcharov 2006) is currently the largest source of barycentric radial velocities of stars (V_r) that are fairly free from systematic errors. It contains V_r for 35 493 stars from the Hipparcos catalogue (the first version – ESA (1997); the new version – van Leeuwen (2007)). The distribution of these stars on a Hertzsprung – Russell (H–R) diagram, for example, of the form “color – absolute magnitude”, corresponds to the distribution of all Hipparcos stars. The median accuracy of V_r from the PCRV is 0.7 km s^{-1} ; for all stars, V_r is more accurate than 5 km s^{-1} . The PCRV includes V_r from 203 catalogues. The two largest present-day catalogues are among them: the Geneva–Copenhagen survey of more

than 14 000 stars mostly of types FV–GV near the Sun (GCS) (Nordström et al. 2004; Holmberg et al. 2007, 2009) and the kinematic survey of more than 6000 KIII–MIII stars based on CORAVEL observations (Famaey et al. 2005).

The desire to minimize the systematic errors of the trigonometric parallaxes due to the Lutz–Kelker and Malmquist biases (Perryman 2009, pp. 209–211) forces us to limit the sample of stars in parallax: $\pi > 3$ milliarcseconds (mas).

Having supplemented the data on V_r and π with the coordinates α and δ and proper motions μ from the new version of Hipparcos, we calculate the complete set of $XYZUVW$ for 26 399 stars.

The accuracy of the components $\mu_\alpha \cos \delta$ and μ_δ for the overwhelming majority of sample stars is higher than 3 mas yr^{-1} . At a distance of 333 pc, this corresponds to an accuracy of 5 km s^{-1} for the velocity components. The accuracy of the V_r used is also higher than 5 km s^{-1} . Thus, the sample is homogeneous with regard to the accuracy of U , V , and W .

The dereddened color $(B_T - V_T)_0$ was calculated for each star:

$$(B_T - V_T)_0 = (B_T - V_T) - E(B_T - V_T), \quad (1)$$

where the reddening $E(B_T - V_T) = A_{V_T}/R_V = 1.1A_V/R_V$ and the extinction A_V , in turn, was calculated from the 3D analytical extinction model (see Gontcharov 2009, 2012b) as a function of the trigonometric distance $r = 1/\pi$ and Galactic coordinates l and b , while the extinction coefficient R_V was calculated from the 3D map of its variations as a function of the same coordinates (Gontcharov 2012a). The absolute magnitude M_{V_T} was calculated for each star from the formula

$$M_{V_T} = V_T + 5 - 5 \lg r - A_{V_T}. \quad (2)$$

Although below we consider only early-type MS stars ($(B_T - V_T)_0 < 0.7$), thick-disk and halo stars (for example, the hot and cool subdwarfs considered by Gontcharov et al. (2011)) are also encountered among them. Here, we consider only Galactic thin-disk stars. We assigned 15 730 sample stars with $(B_T - V_T)_0 < 0.7$ to the thin disk, the thick disk, or the halo in agreement with the criteria from the Besancon model of the Galaxy (BMG) (Robin et

al. 2003):

$$\begin{aligned}\bar{U} - 3\sigma_U &< U < \bar{U} + 3\sigma_U, \\ \bar{V} - 3\sigma_V &< V < \bar{V} + 3\sigma_V, \\ \bar{W} - 3\sigma_W &< W < \bar{W} + 3\sigma_W,\end{aligned}$$

where $\bar{U} = -10$, $\bar{V} = -10 + 0.84e^{3.86(B_T - V_T)_0}$ (this dependence is justified below), and $\bar{W} = -7$ are the mean values of U , V , W for all stellar populations; σ_U , σ_V , σ_W are the boundary velocity dispersions for the three populations. We assigned 15 402 stars with $\sigma_U = 43.1$, $\sigma_V = (27.8^2 + 14.8^2)^{1/2}$, $\sigma_W = 24$ km s⁻¹ to the thin disk, 214 stars with $\sigma_U = 67$, $\sigma_V = (51^2 + 49^2)^{1/2}$, $\sigma_W = 42$ km s⁻¹ to the thick disk, and the remaining 114 stars to the halo; σ_V is the quadratic sum of the dispersion proper (the first term) and the asymmetric drift (the second term), a systematically different Galactic rotation velocity for different populations. In contrast to the BMG, we chose $\sigma_W = 24$ instead of 17.5 km s⁻¹ for the thin disk and an asymmetric drift of 49 instead of 53 km s⁻¹ for the thick disk. These differences are attributable to the distribution of the 15 730 stars under consideration in U , V , and W shown in Fig. 1: the local minima and changes in the smooth behavior of the curve point to the population boundaries.

The thick-disk and halo stars account for 1.4% and 0.7% of the sample, respectively. In the BMG, these ratios are 3.3% and 0.02% for stars of all ages, with the exception of white dwarfs. Since there should be fewer thick-disk and halo stars among the O–F stars and among the G–M ones, their fraction in the sample under consideration appears plausible.

CALCULATING THE AGES

The age of a star is usually estimated from its position on the H–R diagram relative to the theoretical isochrones. Since the isochrones differ significantly for stars of different metallicities in many regions of the H–R diagram, it is desirable to know the stellar metallicity in advance and to consider the set of isochrones for this metallicity. The ages of stars in the GCS were estimated precisely in this way. The metallicity was determined from narrow-band Strömgren photometry. Unfortunately, Strömgren photometry and the calibrations allowing the ages to be estimated from it are available mostly for dwarfs older than 2 Gyr, which were investigated in the GCS. There are almost

no stars younger than 1 Gyr in the GCS. Since the sought-for variations of kinematics with age can be smoothed out and disappear, it is more fruitful to search for them in young stars. Therefore, instead of Strömgren photometry, we use Hipparcos/Tycho-2 photometry (Høg et al. 2000) in the broad B_T and V_T bands to estimate the ages and consider not the individual ages but the mean ones for the sets of stars. Naturally, in order that the concepts of mean age and mean metallicity be meaningful, we will consider only the regions of the H–R diagram where the scatter of these quantities is small. In addition, we will exclude the regions of the H–R diagram where the isochrones for different metallicities are far from each other from consideration.

Figure 2 shows the correlation between dereddened color $(B_T - V_T)_0$ and age from the GCS for the 8795 thin-disk stars under consideration. The solid curve indicates an exponential fit to these data for age T (Gyr):

$$T = 0.41e^{3.9(B_T - V_T)_0}. \quad (3)$$

The relative accuracy of the GCS ages lies predominantly within the range 40–70% and causes a large scatter of ages seen in the figure and even the presence of ages older than the presumed age of the Universe. The scatter of true ages is apparently smaller and using the mean age is justified in the entire range $(B_T - V_T)_0 < 0.65^m$ (in our calculations, we also used stars with $0.65^m < (B_T - V_T)_0 < 0.7^m$, but their kinematics is not considered). This limitation implies the selection of O–G2 stars (hotter and mostly younger than the Sun).

The positions of the stars under consideration on the H–R diagram are shown in Fig. 3 before $((B_T - V_T) - M_{V_T})$ and after $((B_T - V_T)_0 - M_{V_T})$ dereddening. The cross indicates typical errors for an individual star: $\sigma(B_T - V_T) = 0.02$ and $\sigma(M_{V_T}) = 0.5^m$. The curves indicate the isochrones of solar metallicity ($FeH = 0$) stars for ages of 0.001, 0.1, 0.2, 0.4, 1, 2, 3, and 4 Gyr. The 0.001-Gyr isochrone may be considered the zero-age main sequence (ZAMS). Here and below, the isochrones were taken from the Padova database (<http://stev.oapd.inaf.it/cmd>; Bertelli et al. 2008; Marigo et al. 2008).

We see from Fig. 3 that the applied 3D extinction model successfully placed the stars into the expected region of the diagram, predominantly between the ZAMS and the loops of isochrones implying the beginning of the subgiant stage (hydrogen burning in the shell above an inert helium core). We also see that there are almost no giants and low-metallicity stars

(below the ZAMS) among the thin-disk stars in the range $(B_T - V_T)_0 < 0.7^m$. The latter fact can also be seen in the GCS: the mean metallicity for dwarfs with an age of 5 Gyr from the GCS is $\overline{FeH} \approx -0.15$ (while the universally accepted boundaries between the thin disk, the thick disk, and the halo are $FeH \approx -0.4$ and $FeH \approx -1.3$).

We see from Figs. 2 and 3 that there is a strong correlation between age, dereddened color, and metallicity for early-type MS stars pointed out by the GCS authors. According to the GCS, the age dependence of FeH can be represented with an adequate accuracy by the linear trend $\overline{FeH} = 0.01 - 0.034 \cdot T$, or, given dependence (3),

$$\overline{FeH} = 0.01 - 1.394e^{3.9(B_T - V_T)_0}. \quad (4)$$

Using this dependence, we find that only for stars older than 2 Gyr are the \overline{FeH} isochrones offset from the $FeH = 0$ isochrones on the H–R diagram by more than the accuracy of the photometry used. Even for the oldest stars under consideration, the shift of the \overline{FeH} isochrone from the $FeH = 0$ isochrone is $(\Delta((B_T - V_T)_0) < 0.06^m, \Delta(M_{V_T}) < 0.2^m)$, i.e., less than the above mean stellar position error on the H–R diagram due to the parallax error. Therefore, the change in FeH during the last 5 Gyr has almost no effect on the stellar ages calculated below.

The Padova database allows us to interpolate the isochrones with a high accuracy and to unambiguously select the isochrone for each star under consideration by taking into account the metallicity adopted for the star using Eq. (4). Thus, we calculated the individual ages for all stars in the range $(B_T - V_T)_0 < 0.7^m$. However, since they are based on the relations between mean quantities, below they are not used separately but are averaged for the set of stars. We found the mean dependence of the age on dereddened color from the ages calculated in this way:

$$T = 0.42e^{3.86(B_T - V_T)_0}, \quad (5)$$

It agrees well with the analogous dependence (3) for the GCS ages, and these curves coincide on the scale of Fig. 2. Although this coincidence for $(B_T - V_T)_0 > 0.45^m$ is partly explained by the use of dependence (4) to estimate the ages, the age estimates in the remaining range are independent, and we see good agreement between the ages derived here and GCS ages. Thus, although the accuracy of the derived ages (predominantly 50–100%) is lower than that of the GCS ones (40–70%) and they can be used only in

averaging for the set of stars, we see that broad-band photometry can replace narrow-band one in this case.

KINEMATICS

When analyzing the distribution of stars in the UV plane, we divided the sample of 15 402 thin-disk stars into several age subsamples. When the age dependence of the remaining kinematic parameters (dispersions $\sigma(U)$, $\sigma(V)$, $\sigma(W)$, Ogorodnikov–Milne model parameters, Oort constants A , B , C , K , and solar motion components U_\odot , V_\odot , W_\odot) is analyzed, modern computers allow a moving calculation to be applied instead of calculations for a few subsamples. The stars are arranged by age and the mean age, along with the kinematic parameters, is calculated for 1000 minimum-age stars. The minimum-age star is then excluded from the set of stars under consideration, a previously unused minimum-age star is then introduced instead of it, and the calculations of the mean age and kinematic parameters are repeated. As a result, we obtain $15402 - 1000 = 14402$ mean ages with the corresponding set of kinematic parameters. The window of calculations with a width of 1000 stars corresponds to the range of ages from 0.1 Gyr for the youngest stars to 1 Gyr for stars with an age of 5 Gyr.

Age Dependence of the Velocity Dispersion

The variations in dispersions $\sigma(U)$, $\sigma(V)$, $\sigma(W)$ with age for 15 402 thin-disk stars are indicated in Fig. 4 by the solid black curve. The gray band along the black curve indicates the range of errors. We see that some of the dispersion fluctuations around the gradual increase exceed the errors and, therefore, are real (for a discussion, see below).

The gradual increase in dispersions is well (the correlation coefficients are more than 0.97) fitted by power laws, which are indicated in Fig. 4 by the dashed lines: $\sigma(U) = 22.41T^{0.307}$, $\sigma(V) = 14.39T^{0.239}$, $\sigma(W) = 10.26T^{0.353}$. Holmberg et al. (2009) also found a power-law increase in dispersions with age based on GCS data and interpreted it as continuous kinematic “heating” of the thin disk during its lifetime, for example, by the radial migration of metal-poor stars from the inner (with respect to the Sun) Galactic regions according to the theory of Schönrich et al. (2010). It follows from this theory that the kinematic parameters considered here should depend not on age but

on metallicity. The observed age–metallicity correlation does not yet allow us to decide what argument the variations of kinematics depend on. It is also possible that both views are correct: the radial migrations of metal-poor stars affect the kinematics in some periods, while other mechanisms increasing the velocity dispersion with age irrespective of the metallicity affect it in the remaining time.

The stepwise polygonal curves in Fig. 4 indicate the dependences adopted in the BMG from the results of Gomez et al. (1997). We see that these steps are a rather rough approximation of the gradual increase in dispersions, but, on average, the derived $\sigma(U)$ corresponds to the BMG, $\sigma(V)$ is appreciably smaller, and $\sigma(W)$ for old stars is larger than that in the BMG. Gomez et al. (1997) used π and μ from Hipparcos, dissimilar V_r , a set of isochrones, Strömgren photometry, and other data that, on the whole, are inferior to our data in accuracy and the number of stars: for example, the limiting accuracy of U , V , and W is 15 km s^{-1} against 5 km s^{-1} , the number of stars younger than 5 Gyr is about 1500 against 14 350. Consequently, the inaccuracy and incompleteness of the data by Gomez et al. is the most likely cause of the discrepancy in dispersion estimates. In particular, the discrepancy in $\sigma(W)$ is explained by the difference in estimating the kinematic boundary of the thin and thick disks: 24 km s^{-1} here instead of 17.5 km s^{-1} in the BMG. It can be seen from Fig. 1 that, having adopted the lower value, we lose the fast old thin-disk stars. Obviously, they were lost by Gomez et al. due to the low accuracy of V_r , because the old stars located mostly comparatively far from the Galactic plane have comparatively large V due to Galactic rotation and small W in this case, erroneous V_r give a large relative error of W and, in combination with large V , this increases the probability of assigning an erroneously large total velocity to a star and classifying it as a thick-disk or halo star. The opposite discrepancy in V is explained in the same way: here, erroneous V_r give a large relative error of V that is canceled out by large V and the thick-disk stars with small μ , U and W are erroneously considered thin-disk ones.

The individual symbols with error bars in Fig. 4 indicate the extraneous results: the gray squares – Dehnen and Binney (1998), the result was obtained only from μ ; the gray circles – Francis and Anderson (2009); the gray diamonds – Torra et al. (2000); the black triangles – Mignard et al. (2000), the result was obtained only from μ ; the black diamonds – Chen et al. (1997); the black squares – Gontcharov (2011); the black circles – Famaey et al. (2005). All these results are in agreement with those obtained here,

although it should be noted that many of these results are not completely independent, because the data from the same sources are used everywhere, while V_r with corrected systematic errors for stars over the entire sky are used only in Gontcharov (2011) and this study.

Famaey et al. (2005) and Gontcharov (2011) obtained their results for red giant branch KIII and MIII stars with presumed ages from 3 to 10 Gyr. Here, arbitrary ages of 4.7 and 4.9 Gyr for KIII and MIII stars, respectively, were assigned to them, and they point out an almost constant dispersion level for stars older than 4.5 Gyr. This absence of an increase in dispersion for old stars at a noticeable increase for young ones is known as the Parenago (1950) discontinuity. It was considered in detail by Dehnen and Binney (1998); according to them, the dispersions are stabilized at $(B_T - V_T)_0 \approx 0.61^m$, i.e., according to Eq. (5), at an age of about 4.4 Gyr. They offered a possible, though not conclusively proven explanation: the color correlates with the age for O–F dwarfs and subgiants and does not correlate for G–M, with the boundary lying near the color for which the lifetime of a star near the MS is equal to the lifetime of the Galactic disk, i.e., 10 Gyr for solar-type stars. This is because there are no old stars among the OF dwarfs and subgiants, while the G–M dwarfs and subgiants are distributed in ages from 0 to 10 Gyr rather uniformly. It is important that the color–age correlation pointed out by Dehnen and Binney underlies the method applied in this paper. Therefore, in fact, the kinematics of dwarfs and subgiants bluer than the color at which the Parenago discontinuity manifests itself is considered here.

Dehnen and Binney (1998) and Mignard (2000) obtained their results using only μ , without V_r . Their systematic deviation to lower values from $\sigma(U)$ and $\sigma(W)$ obtained here appears to be explained in the same way as the smaller $\sigma(W)$ in the BMG was explained previously: Galactic rotation dominating in the motion of stars for the velocity components U and W manifests itself mainly in μ , and the remaining motions in U and W are difficult to reveal against the background of Galactic rotation without invoking V_r .

The vertical arrows in Fig. 4a indicate four distinct periods of sharp $\sigma(U)$ spikes against the background of a gradual rise: about 0.6, 1.2, 2.3, and 3.1 Gyr ago. The same $\sigma(U)$ spikes are seen in the results of Dehnen and Binney (1998) (gray squares), Francis and Anderson (2009) (gray circles), and Gomez et al. (1997) (absent in the figure). As we show below, when the distribution of stars in the UV plane is analyzed, the sharp increase in $\sigma(U)$ is caused by the formation or intrusion of stellar streams in the region of space under consideration. Since no sharp increase in dispersion manifested

itself in these periods or it was indistinct in Figs. 4b and 4c, these streams have a predominantly radial direction (along the X axis).

Figure 5 shows the age dependence for the shape of the velocity ellipsoid, i.e., for the dispersion ratios $\sigma(V)/\sigma(U)$ (black solid curve) and $\sigma(W)/\sigma(U)$ (gray solid curve) in comparison with the same quantities from the BMG (the black and grays dashed curves, respectively). The deviation of our result from the BMG is explained by the systematic difference between $\sigma(V)$ and $\sigma(W)$ mentioned above. The influence of the radial streams is also seen in these results as the periods of a decrease in both ratios. The overall pattern of the curves suggests a strong deviation of the velocity distribution from the theoretically justified ellipsoid for stars younger than 0.6 Gyr and stabilization of these ratios for stars older than about 1.5 Gyr at $\sigma(V)/\sigma(U) \approx 0.6$ and $\sigma(W)/\sigma(U) \approx 0.5$. The results by Gomez et al. (1997) show the same for stars younger than 1.5 Gyr, but stabilization for old stars occurs at 0.7 and 0.62, respectively. Famaey et al. (2005) obtained, on average, about 0.65 and 0.5 for old red giant branch stars, i.e., close to the stabilization levels of these quantities obtained here. Their simulations gave 0.79 and 0.55, which differ from the empirical ones due to selection in favor of slow stars because of sample incompleteness. Gontcharov (2011) and Bobylev et al. (2009) pointed out the variations in these ratios with coordinate Z . Thus, there is a great variety of estimates, but, as has been noted above, the accuracy and volume of the data used are primarily important. Therefore, the values obtained here appear most plausible.

Distribution of Stars in the UV Plane

The distribution of the selected thin-disk stars in projection onto the UV plane is shown in Fig. 6. In this case, the sample was divided into the following subsamples to reveal the streams: (a) 2244 stars younger than 0.4 Gyr, (b) 1938 stars with ages 0.4–0.9 Gyr, (c) 3062 stars with ages 0.9–1.9 Gyr, (d) 3332 stars with ages 1.9–2.8 Gyr, (e) 1875 stars with ages 2.8–3.6 Gyr, and (f) 1899 stars with ages 3.6–5 Gyr. In support of the reality of the calculated ages, the main known superclusters (dynamical streams) appear and disappear in the graphs in complete agreement with the theoretical and empirical results by Antoja et al. (2008) presented in their Fig. 13, Fig. 6a is consistent with their graph for stars with ages 0.1–0.5 Gyr, Figs. 6b and 6c are consistent with their graph for stars with ages 0.5–2 Gyr, etc., as well as with the empirical results by Francis and Anderson (2009) presented in

their Fig. 9. The main streams are (the mean values of U , V , and W were taken from Antoja et al. (2008) and Bobylev et al. (2010)): the Pleiades ($U \approx -14 \text{ km s}^{-1}$, $V \approx -23 \text{ km s}^{-1}$) becomes smaller in the number of members than other streams in accordance with the age of the cluster itself, about 100 Myr (Bovy and Hogg 2010); Coma Berenices ($U \approx -11 \text{ km s}^{-1}$, $V \approx -8 \text{ km s}^{-1}$) becomes inferior to the Pleiades in the number of members with age; the streams NGC 1901 ($U \approx -25 \text{ km s}^{-1}$, $V \approx -10 \text{ km s}^{-1}$) and IC 2391 ($U \approx -21 \text{ km s}^{-1}$, $V \approx -16 \text{ km s}^{-1}$) are particularly clearly seen in Figs. 6a and 6b not far from the Pleiades and Coma Berenices, being lost near the Hyades in Figs. 6c–6f, which is in agreement with the age of the cluster NGC 1901 itself, $0.4 \pm 0.1 \text{ Gyr}$ (Carraro et al. 2007); the Sirius or Ursa Major stream ($U \approx +9 \text{ km s}^{-1}$, $V \approx +3 \text{ km s}^{-1}$) is more clearly seen in Figs. 6b–6d at an estimated age of the cluster itself 350–413 Myr (Bovy and Hogg 2010); the Hyades ($U \approx -43 \text{ km s}^{-1}$, $V \approx -20 \text{ km s}^{-1}$) manifests itself in Figs. 6c–6e at an estimated age of the cluster itself 488 – 679 Myr (Bovy and Hogg 2010); the α Ceti or Wolf 630 stream ($U \approx +23 \text{ km s}^{-1}$, $V \approx -28 \text{ km s}^{-1}$) appears in Figs. 6d–6f in accordance with the results by Francis and Anderson (2009) and Bobylev et al. (2010); the Hercules stream ($U \approx -30 \text{ km s}^{-1}$, $V \approx -50 \text{ km s}^{-1}$) is represented by a few stars in Fig. 6c and contains an increasing large fraction of stars when passing from Fig. 6d to Fig. 6f; the HR 1614 stream ($U \approx +15 \text{ km s}^{-1}$, $V \approx -60 \text{ km s}^{-1}$) can be seen only in Fig. 6f, i.e., for an age of more than 3.5 Gyr ago in accordance with the analysis by Bobylev et al. (2010).

Comparison of Figs. 6 and 4 shows that the $\sigma(U)$ spikes marked by the arrows in Fig. 4a were caused about 0.6, 1.2, 2.3, and 3.1 Gyr ago mainly by the Sirius, Hyades, α Ceti/Wolf 630, and Hercules streams, respectively, although other streams also play some role in all cases.

Solar Motion Relative to the Stars

The solar velocity components U_{\odot} , V_{\odot} , W_{\odot} are plotted against the stellar age in Fig. 7: the black curve with the gray error band represents our result for 15 402 thin-disk stars. This result agrees, within the error limits, with most of the extraneous results marked in the figure by individual symbols: the gray squares – Dehnen and Binney (1998), the result was obtained only from μ ; the gray circles – Francis and Anderson (2009); the gray diamonds – Torra et al. (2000); the black triangles – Mignard (2000), the result was obtained only from μ ; the black diamonds – Chen et al. (1997); the black

squares – Gontcharov (2011); the black circles – Famaey et al. (2005); the gray triangles – Zhu (2000); and the black stars – Mendez et al. (2000). We see reliably determined smooth variations in solar motion, with those in W_{\odot} being possibly periodic, with a period of ~ 1 Gyr. The stable motion 2 – 5 Gyr ago changed abruptly to a stable motion in a slightly different direction 0.9 – 1.7 Gyr ago, and in the last 0.5 Gyr the motion changed most significantly over all 5 Gyr. Naturally, not the solar motion but the composition of the sample of stars serving as a frame of reference or a realization of the local standard of rest (LSR) changes. These changes result, for example, from the appearance of the previously mentioned radial stellar streams in the solar neighborhood under consideration and from the deformation and displacement of the layer of star-forming gas (for example, in the Gould Belt in the last 0.1 Gyr, according to Gontcharov (2009, 2012c)).

The shape of the curve in Fig. 7b reflects a smooth variation in the revolution velocity of stars around the Galactic center with their age – an asymmetric drift: the stars born later revolve more rapidly, but the Sun overtake them as well. Many studies are devoted to determining this peculiar solar motion. Their results disagree mainly because the researchers refuse to recognize the obvious dependence of the solar motion on stellar age and because there is disagreement in choosing “reference” stars for the LSR.

For example, the dashed straight line in Fig. 7b indicates the fit to the asymmetric drift from Dehnen and Binney (1998) for stars older than 0.5 Gyr (over the gray squares, except the two leftmost ones). For imaginary zero-age stars it gives $V_{\odot} = 5.25 \text{ km s}^{-1}$ widely used by researchers (more than 600 references) and marked in the graph by the snowflake. In reality, however, there are no zero-age stars and, in general, no sufficient number of stars revolving so rapidly around the Galactic center for LSR realization. The attempts to find their analogs among the youngest stars fail due to the peculiarity of the motion of the latter in the Gould Belt seen in Figs. 7a and 7b: the youngest stars are not the ones revolving most rapidly around the Galactic center. Instead of the imaginary zero-age stars, Schönrich et al. (2010) proposed to use real stars with the maximum revolution velocity around the Galactic center by assuming them to be, on average, the most metal-rich ones and by replacing the age dependence by the metallicity dependence. These turned out to be stars with ages of about 0.5 Gyr: the arrow and the second snowflake in Fig. 7b mark the transfer of the Dehnen–Binney LSR by Schönrich et al. However, there is an uncertainty here due to the membership of stars in streams as well. It is reflected the estimated

systematic error of the result by Schönrich et al. -2 km s^{-1} at a random error of only 0.5 km s^{-1} .

The failed attempts to use young stars as a realization of the LSR forced the researchers to turn to old red giants, but Famaey et al. (2005) detected stellar streams here as well and directly cast doubt on the presence of some set of stars having no net radial motion in the solar neighborhood which can be used as a reference against which to measure the solar motion.

However, it can be seen from Fig. 7b that the values of V_{\odot} are nevertheless grouped near some smooth curve that should be close to our results. This means that we can produce a sample of stars with a *known age* relative to which the solar motion can be determined with an accuracy, say, of about 0.2 km s^{-1} . The systematic motions of stars only set some insurmountable limit for this accuracy and make the determinations of the solar motion without specifying the ages of the stars realizing the LSR completely meaningless.

Kinematics According to the Ogorodnikov–Milne Model

Let us determine the kinematics of the subsamples within the linear Ogorodnikov–Milne model described by Gontcharov (2011): let us calculate the partial derivatives of the velocity with respect to the distance M_{ux}, \dots, M_{wz} (including the angular velocity of Galactic rotation $\Omega_{R0} = -M_{uy}$), the Oort constants A, B, C, K , and the vertex deviation l_{xy} . The distances are an additional source of errors not only because the accuracy of the parallaxes is limited but also because the old stars of the sample under consideration are rather faint and are in a very small solar neighborhood, for example, the stars with an age of 2 Gyr within 50 pc rather than 333 pc of the Sun. A small range of distances gives large errors when calculating the partial derivatives of the velocity with respect to the distance. Therefore, let us consider the variations in model parameters only during the last 2 Gyr. They are shown in Fig. 8 together with the error bands. The variations in M_{wx} and M_{wy} are insignificant. All the time, except the last 0.3 Gyr, the variations in M_{vx}, M_{wz} and A are also insignificant. The variations in M_{ux}, M_{uy} and M_{uz} , caused by the mentioned radial streams are most significant. Sharp transitions from one prolonged state to another are seen.

For example, about 1.3 Gyr ago, the formation or intrusion of the Hyades disturbed the calmness in the solar neighborhood and changed the following quantities for a long time: l_{xy} from 0 to $+15^{\circ}$, B from -5 to $-20 \text{ km s}^{-1} \text{ kpc}^{-1}$ (the local motions dominate over the involvement of stars in Galactic

rotation), C from 0 to $-10 \text{ km s}^{-1} \text{ kpc}^{-1}$, the Galactic rotation velocity ($-M_{uy}$) from -20 to $-40 \text{ km s}^{-1} \text{ kpc}^{-1}$, M_{vy} from -5 to $+10 \text{ km s}^{-1} \text{ kpc}^{-1}$ (the slight compression of the set of stars along the Y axis is replaced by a strong expansion), M_{vz} from 0 to $-15 \text{ km s}^{-1} \text{ kpc}^{-1}$ (the Hyades moves below the Galactic plane in the direction of Galactic rotation), the prolonged decrease in M_{uz} is replaced by a prolonged increase (the Hyades moves below the Galactic plane toward the Galactic anticenter), and M_{vx} becomes zero for a long time.

Here is another example. About 0.25 Gyr ago, the processes that subsequently produced the Gould Belt began (the last 0.18 Gyr are not considered here, but they were analyzed by Gontcharov (2012c)): M_{ux} changes from -15 to $+5 \text{ km s}^{-1} \text{ kpc}^{-1}$ (the compression along the X axis is replaced by expansion), M_{vz} and M_{wy} change from -15 to $-20 \text{ km s}^{-1} \text{ kpc}^{-1}$ and from 0 to $+5 \text{ km s}^{-1} \text{ kpc}^{-1}$, respectively, both changes imply the emergence of rotation around the X axis, B changes from -10 to $-15 \text{ km s}^{-1} \text{ kpc}^{-1}$ (the local motions increase in importance), C changes from -10 to $+5 \text{ km s}^{-1} \text{ kpc}^{-1}$, and K changes from -8 to $0 \text{ km s}^{-1} \text{ kpc}^{-1}$ (the prolonged compression ceases).

CONCLUSIONS

For a sample of 15 730 O–F stars with accurate α , δ , μ , and $\pi > 3$ mas from the new version of Hipparcos and V_r from the PCRV, we calculated the complete set of position and motion components X , Y , Z , U , V , W , with the accuracy of U , V , and W being higher than 5 km s^{-1} . The sample was divided into 15 402 thin-disk stars, 214 thick-disk stars, and 114 halo stars. We showed that the W range for the thin-disk stars should be wider than that in the Besancon model of the Galaxy.

The ages for the thin-disk stars independent of X , Y , Z , U , V , W were calculated from their positions on the $(B_T - V_T)_0 - M_{V_T}$ diagram relative to the isochrones from the Padova database for the mean metallicity for a given color. $(B_T - V_T)_0$ and M_{V_T} were calculated by taking into account the extinction from the 3D analytical extinction model by Gontcharov (2009) and the extinction coefficient R_V from the 3D map of its variations from Gontcharov (2012a).

We analyzed the variations with age for the velocity dispersions $\sigma(U)$, $\sigma(V)$, $\sigma(W)$, solar motion components U_\odot , V_\odot , W_\odot , Ogorodnikov–Milne model parameters, Oort constants A , B , C , K , vertex deviation l_{xy} , and

the distribution of stars in the UV plane. For all quantities, except the distribution in UV , we applied a moving calculation with a window with a width of 1000 stars.

We found smooth variations of the above kinematic parameters with age consistent with all of the extraneous results for which the stellar ages were determined. The velocity dispersion variations are well fitted by power laws the deviations from which are explained by the short-term influence of predominantly radial stellar streams: Sirius, the Hyades, α Cet/Wolf 630, and Hercules. The derived reconciled variations of the Ogorodnikov–Milne model parameters and Oort constants are also caused mainly by these streams. The accuracy of determining the solar motion relative to the local standard of rest was shown to be fundamentally limited due to the variations of stellar kinematics with age.

Our study showed the possibility of using multicolor broad-band photometry to calculate the ages of stars and, hence, the possibility of a more thorough analysis of the kinematics in future by invoking not thousands of Hipparcos stars but hundreds of thousands of Tycho-2 stars with α , δ , μ , photometric distances (derived, for example, by Gontcharov (2011, 2012c)), which is restrained by the absence of their V_r .

ACKNOWLEDGMENTS

This study was financially supported by Program P21 of the Presidium of the Russian Academy of Sciences, as well as by the Federal programm of the Ministry of education and science of the Russian Federation “Scientific and scientific-pedagogical personnel of innovative Russia”, stage 37, event 1.2.1.

References

1. T. Antoja, F. Figueras, D. Fernandez, et al., *Astron. Astrophys.* **490**, 135 (2008).
2. G. Bertelli, L. Girardi, P. Marigo, et al., *Astron. Astrophys.* **484**, 815 (2008).
3. V.V. Bobylev, A.S. Stepanishchev, A.T. Bajkova, and G.A. Gontcharov, *Astron. Lett.* **35**, 836 (2009).

4. V.V. Bobylev, A.T. Bajkova, A.A. Myullyari, *Astron. Lett.* **36**, 27 (2010).
5. J. Bovy and D.W. Hogg, *Astrophys. J.* **717**, 617 (2010).
6. G. Carraro, R. De la Fuente Marcos, S. Villanova, et al., *Astron. Astrophys.* **466**, 931 (2007).
7. B.Chen, R. Asiain, F. Figueras, et al., *Astron. Astrophys.* **318**, 29 (1997).
8. W. Dehnen and J. Binney, *Mon. Not. R. Astron. Soc.* **294**, 429 (1998).
9. ESA, *Hipparcos and Tycho catalogues* (ESA, 1997).
10. B. Famaey, A. Jorissen, X. Luri, et al., *Astron. Astrophys.* **430**, 165 (2005).
11. C. Francis and E. Anderson, *New Astron.* **14**, 615 (2009).
12. A. E. Gomez, S. Grenier, S. Udry, et al., in *Proceedings of the ESA Symp. "Hipparcos Venice 97"*, ESA SP-402, Ed. by B. Battrock (ESA-Publ.Division, c/o ESTEC, Noordwijk, The Netherlands, 1997), p. 621.
13. G. A. Gontcharov, *Astron. Lett.* **32**, 759 (2006).
14. G. A. Gontcharov, *Astron. Lett.* **35**, 780 (2009).
15. G. A. Gontcharov, *Astron. Lett.* **37**, 707 (2011).
16. G. A. Gontcharov, *Astron. Lett.* **38**, 12 (2012a).
17. G. A. Gontcharov, *Astron. Lett.* **38**, 87 (2012b).
18. G. A. Gontcharov, *Astron. Lett.* **38**, 694 (2012c).
19. G.A. Gontcharov, A.T. Bajkova, P.N. Fedorov, et al., *Mon. Not. R. Astron. Soc.* **413**, 1581 (2011).
20. E. Høg, C. Fabricius, V.V. Makarov, et al., *Astron. Astrophys.* **355**, L27 (2000).
21. J. Holmberg, B. Nordström and J. Andersen, *Astron. Astrophys.* **475**, 519 (2007).

22. J. Holmberg, B. Nordström and J. Andersen, *Astron. Astrophys.* **501**, 941 (2009).
23. F. van Leeuwen, *Astron. Astrophys.* **474**, 653 (2007).
24. P. Marigo, L. Girardi, A. Bressan, et al., *Astron. Astrophys.* **482**, 883 (2008).
25. R.A. Mendez, I. Platais, T.M. Girard, et al., *Astron. J.* **119**, 813 (2000).
26. F. Mignard), *Astron. Astrophys.* **354**, 522 (2000).
27. B. Nordström, M. Mayor, J. Andersen, et al., *Astron. Astrophys.* **418**, 989 (2004).
28. P. P. Parenago, *Astron. Zh.* **27**, 150 (1950).
29. M. Perryman, *Astronomical Applications of Astrometry* (Cambridge Univ. Press, Cambridge, 2009).
30. A.C. Robin, C. Reyle, S. Derriere, et al., *Astron. Astrophys.* **409**, 523 (2003).
31. R. Schönrich, J. Binney and W. Dehnen), *Mon. Not. R. Astron. Soc.* **403**, 1829 (2010).
32. J. Torra, D. Fernandez and F. Figueras, *Astron. Astrophys.* **359**, 82 (2000).
33. Z. Zhu, *Publ. Astron. Soc. Jpn.* **52**, 1133 (2000).

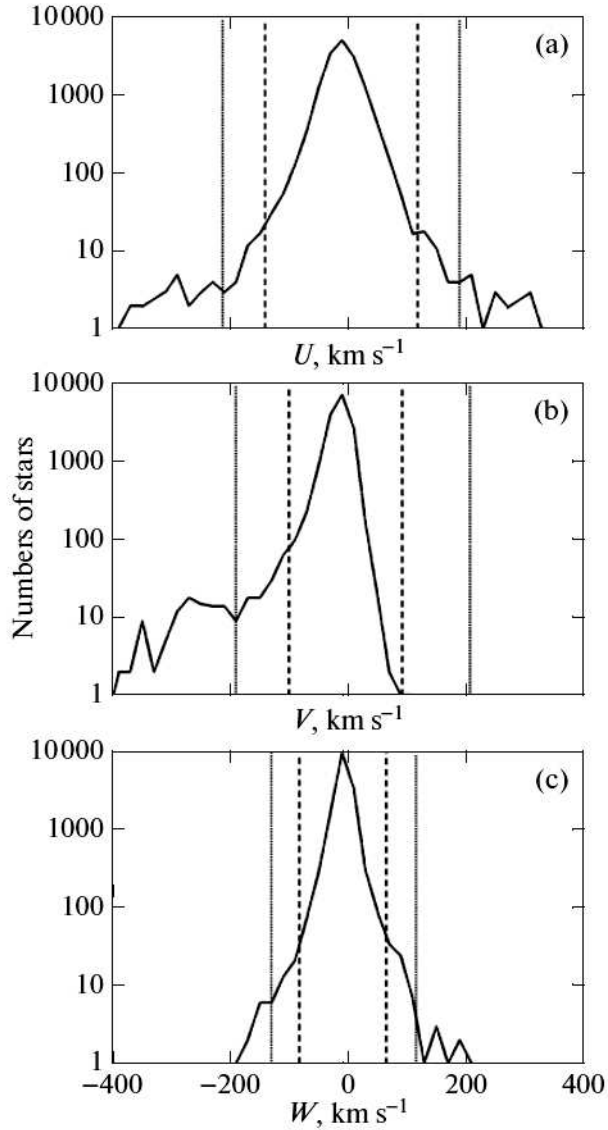


Figure 1: Distribution of 15 730 stars from the initial sample in velocity components U (a), V (b), and W (c). The adopted boundaries of the thin disk, the thick disk, and the halo are indicated by the vertical dashed and dotted straight lines, respectively.

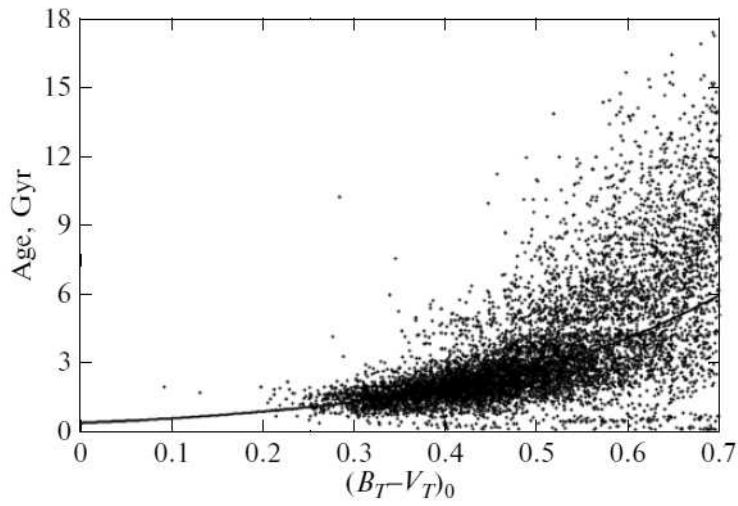


Figure 2: Correlation between dereddened color $(B_T - V_T)_0$ and age from the GCS for 8795 thin-disk stars. The power-law fit (3) to these data is indicated by the solid curve. On the scale of the figure, it coincides with curve (5) fitting the correlation between $(B_T - V_T)_0$ and age calculated here for 15 402 thin-disk stars.

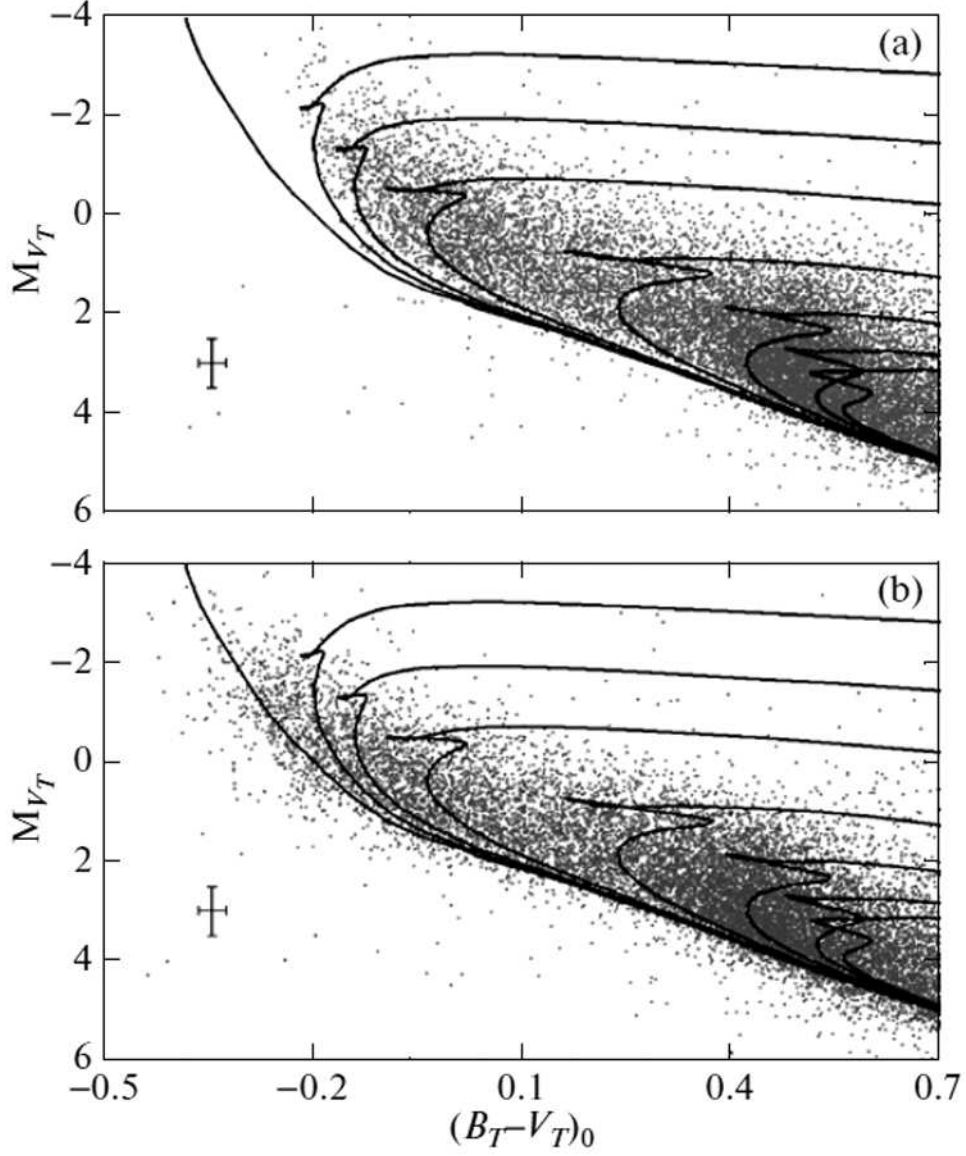


Figure 3: Distribution of the 15 402 thin-disk stars under consideration on the (a) $(B_T - V_T) - M_{V_T}$ (before dereddening) and (b) $(B_T - V_T)_0 - M_{V_T}$ (after dereddening) diagrams. The curves indicate the isochrones for solar-metallicity stars with ages (from left to right) of 0.001, 0.1, 0.2, 0.4, 1, 2, 3, and 4 Gyr. The cross indicates typical errors of $(B_T - V_T)$ and M_{V_T} for an individual star.

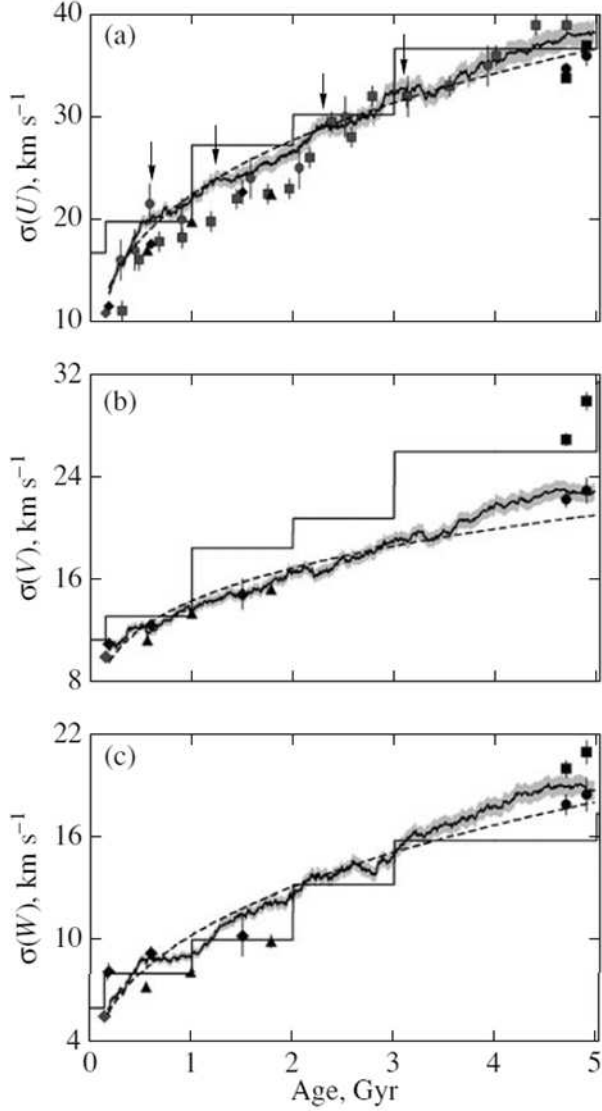


Figure 4: Dispersions $\sigma(U)$ (a), $\sigma(V)$ (b), and $\sigma(W)$ (c) versus stellar age: the black curve with a gray band of errors indicates our result for 15 402 thin-disk stars, the dashed curve is a power-law fit, the stepwise polygonal curve represents the BMG, the individual symbols represent the extraneous results listed in the text, the arrows mark the periods of $\sigma(U)$ growth due to the stellar streams.

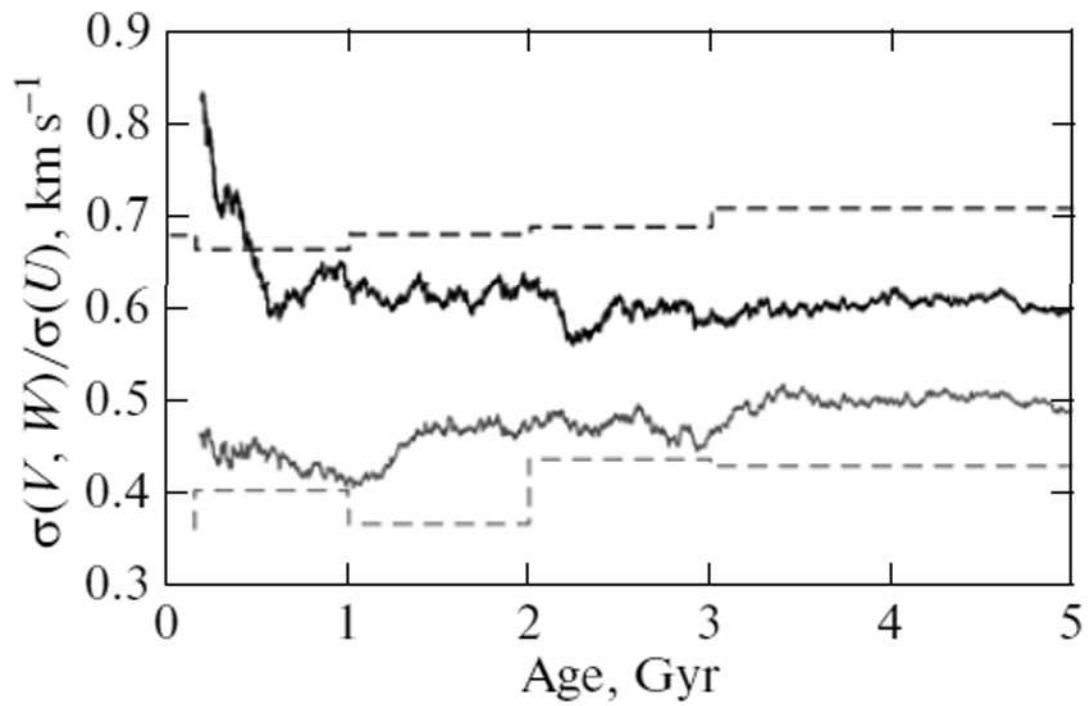


Figure 5: Age dependence of the dispersions $\sigma(V)/\sigma(U)$ and $\sigma(W)/\sigma(U)$ derived here (the black and gray curves, respectively) in comparison with the BMG (the black and gray dashed curves, respectively).

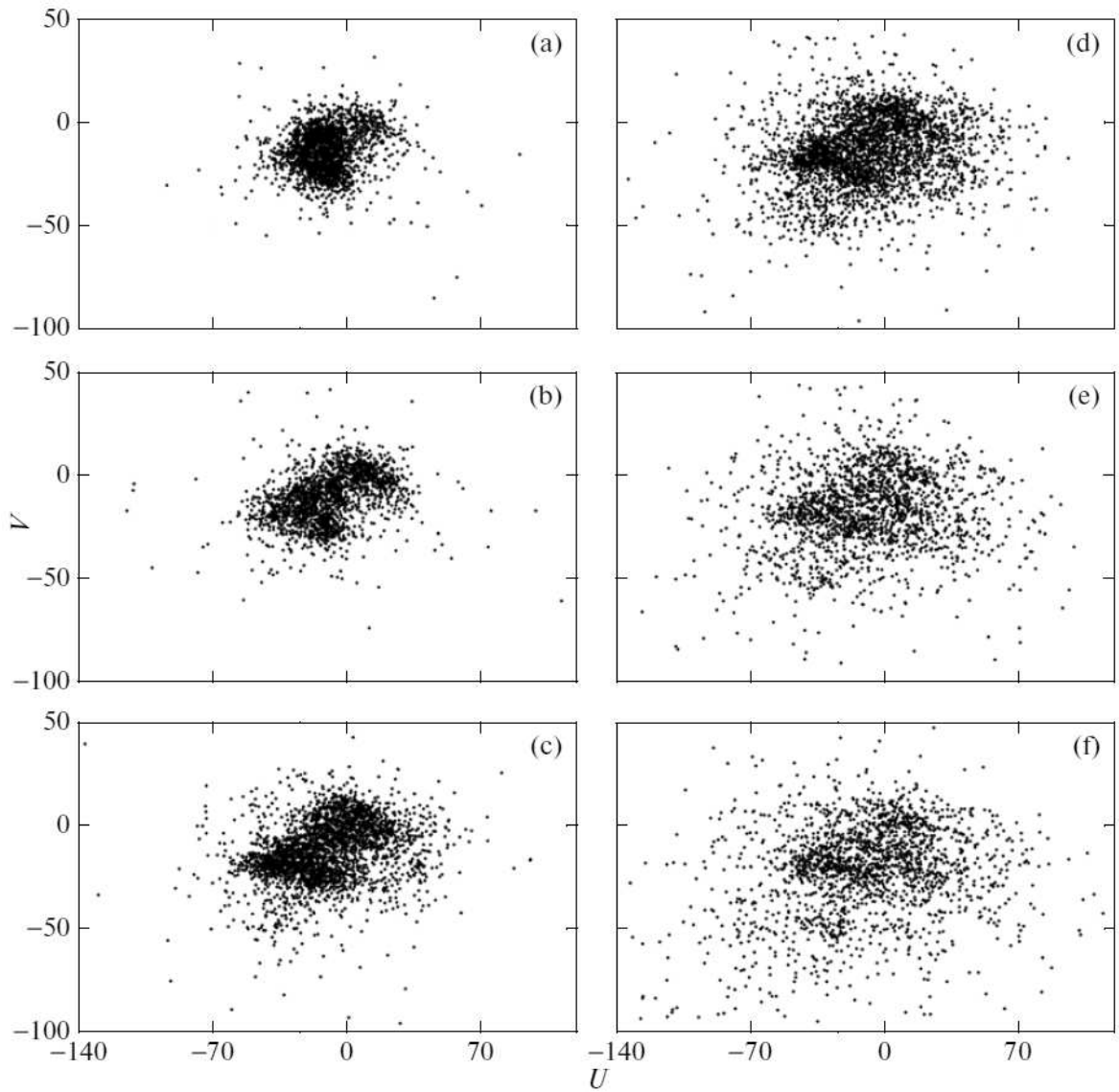


Figure 6: Distribution of thin-disk stars in the UV plane: (a) 2244 stars younger than 0.4 Gyr, (b) 1938 stars with ages 0.4 – 0.9 Gyr, (c) 3062 stars with ages 0.9 – 1.9 Gyr, (d) 3332 stars with ages 1.9 – 2.8 Gyr, (e) 1875 stars with ages 2.8 – 3.6 Gyr, and (f) 1899 stars with ages 3.6 – 5 Gyr.

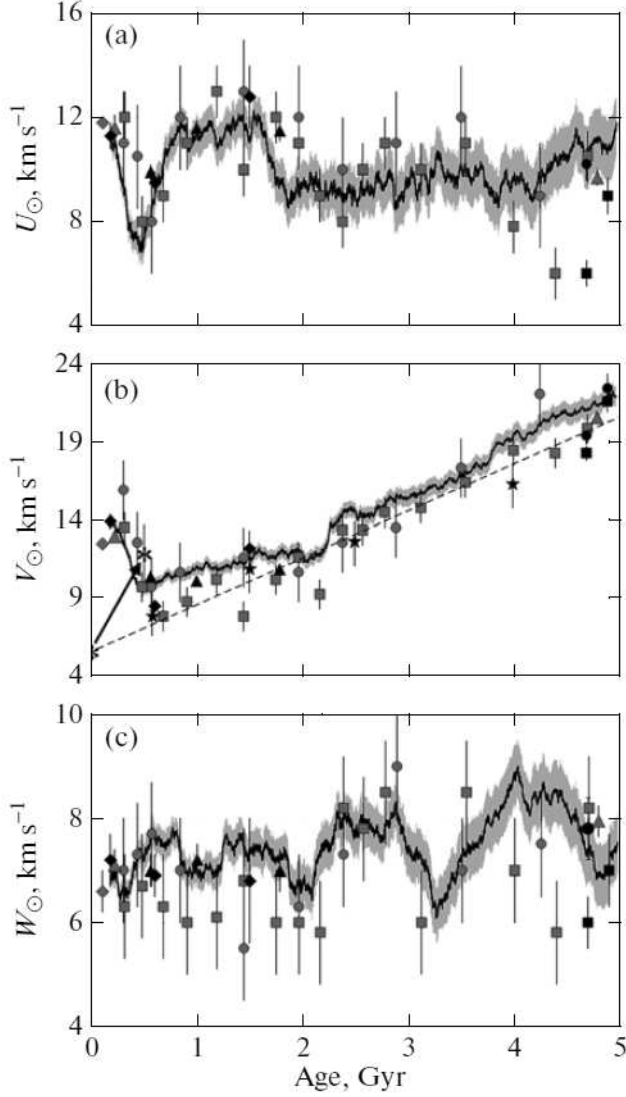


Figure 7: Solar velocity components U_{\odot} (a), V_{\odot} (b), and W_{\odot} (c) versus stellar age: the black curve with the gray error band represents our result for 15 402 thin-disk stars; the individual symbols represent the extraneous results listed in the text. The dashed straight line indicates the fit to the asymmetric drift from Dehnen and Binney (1998), which gives $V_{\odot} = 5.25 \text{ km s}^{-1}$ (snowflake) for their adopted LSR; the arrow and the second snowflake mark the transfer of this value by Schönrich et al. (2010).

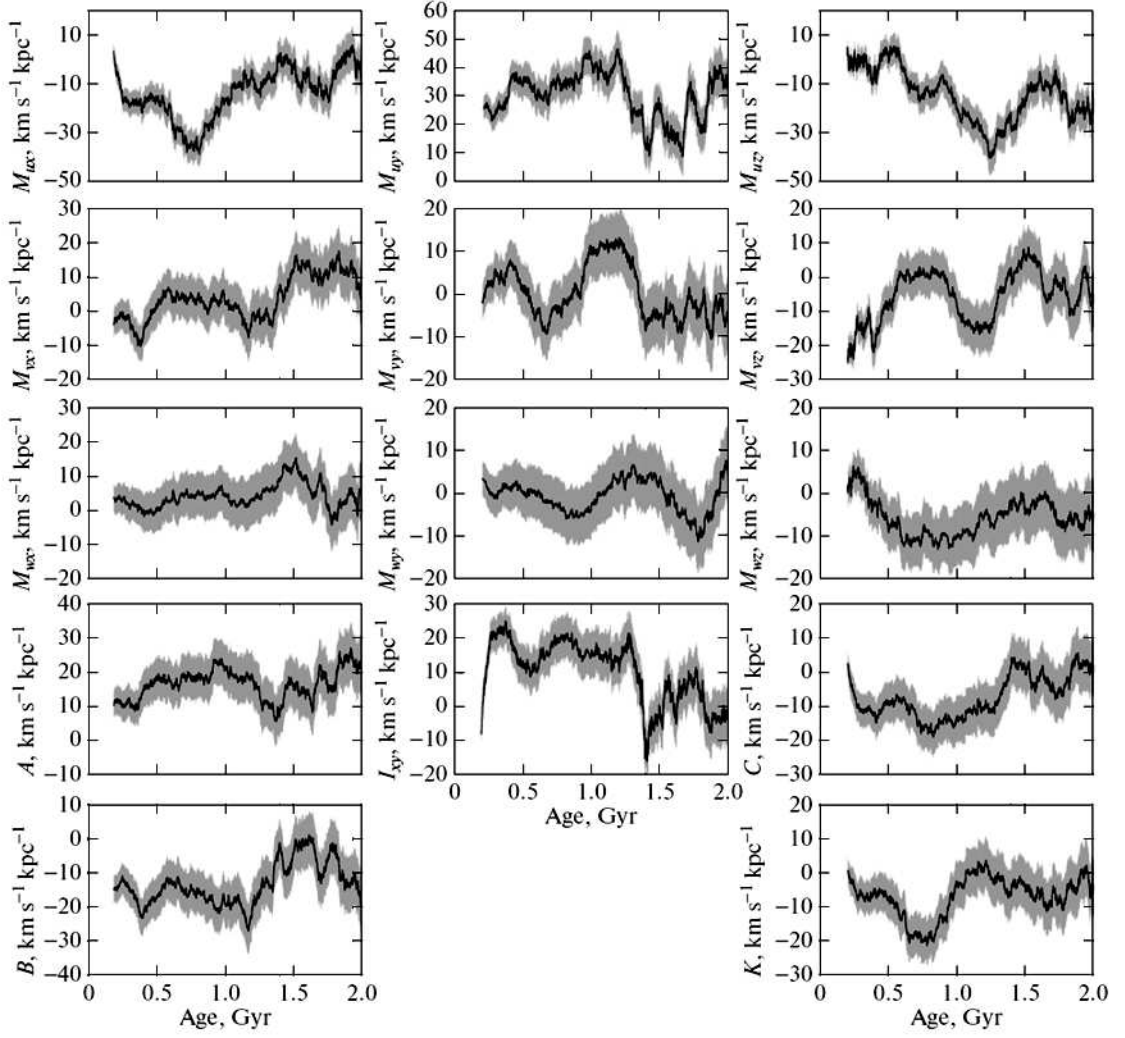


Figure 8: Kinematic parameters of the Ogorodnikov–Milne model for thin-disk stars versus their age.